AIAA JOURNAL
Vol. 43, No. 10, October 2005

Vectoring of Adjacent Synthetic Jets

Barton L. Smith*
Utah State University, Logan, Utah 84322
and
Ari Glezer†
Georgia Institute of Technology, Atlanta, Georgia 30332-0405

The formation, evolution, and interactions of a closely spaced pair of coflowing rectangular synthetic jets are investigated using particle image velocimetry. The dynamics of the combined jet is determined by the interactions of the counter-rotating vortex pairs that form each jet. These vortex pairs are formed along the long edges of the orifice of each jet by the time-periodic motion of a diaphragm that is mounted in a cavity underneath the orifice plate and is driven at resonance. It is shown that the phase between the actuation waveforms of the adjacent jets affects the relative timing between their blowing and suction strokes and consequently the formation of the vortex pairs that synthesize each of the jets. These phase variations also lead to controlled vectoring or bending of the combined jet toward the orifice of the jet that is leading in phase and can be varied dynamically on time scales that correspond to the actuation period.

I. Introduction

In recent years, synthetic jets have attracted considerable attention because of their utility as fluidic actuators in a number of flow control applications. Plane and round synthetic jets are typically formed by time-periodic alternate ejection and suction of the working fluid through an orifice in the flow boundary. Such jets have been investigated in recent years both experimentally (e.g., Smith and Glezer,[1,2] Cater and Soria,[3] and Smith and Swift[4]) and numerically (e.g., Kral et al.[5] and Rizzetta et al.[6]). These investigations have emphasized a compact flow generator in which the orifice forms one of the surfaces of an otherwise sealed cavity where the flow is driven by the motion of a diaphragm (or a piston) that is built into one of the cavity walls. For a given actuation input, the effectiveness of the flow generator can be maximized when the diaphragm and cavity are driven at a coupled resonance that depends on both the cavity acoustics and the structural characteristics of the diaphragm. An important attribute of these jets is that although they have finite streamwise momentum, they have inherently zero net mass flux, and therefore when used as flow actuators, they simplify fluidic packaging and can be easily integrated into complex geometries.

The formation and evolution of two-dimensional synthetic jets was investigated in detail by Smith and Glezer.[1,2] A rectangular jet was formed at a high-aspect-ratio orifice bounding a sealed cavity by the motion of a piezoelectrically driven membrane mounted on the cavity wall. The authors showed that the flowfield of the jet comprises two distinct streamwise domains. In the near field immediately downstream of the orifice ($x/L_0 < 0.2$, where L_0 is the characteristic length of the ejected fluid volume defined in Sec. II), the flow is dominated by the time-periodic alternate formation of counter-rotating vortex pairs that are advected away from the orifice and by suction of the makeup fluid into the cavity. In contrast to conventional jets, the vortices that form the synthetic jet do not coalesce but become unstable and break down to form a second flow regime, a turbulent jet that exhibits many of the characteristics of conventional plane jets. In a recent investigation of a round synthetic jet issuing into a quiescent medium, Cater and Soria[3] compared the evolution of a synthetic jet to a continuous jet that was created in the same apparatus and showed that although the cross-stream velocity distributions of the two jets were similar, the streamwise spreading rate of synthetic jets is larger. A similar comparison of two-dimensional synthetic and conventional jets was also reported by Smith and Swift,[4] who reported the same basic results.

The interaction of a synthetic jet (or jet arrays) with an external cross flow over the surface in which they are mounted can displace the local streamlines and induce an apparent or virtual change in the shape of the surface and is therefore of considerable interest for flow control applications. In an investigation of the evolution of synthetic jets on the surface of a two-dimensional cylinder Honohan et al.[7] and, more recently, Glezer et al.[8] demonstrated that when the jets are operated on a timescale that is well below the characteristic time scale of the base flow, the formation of a quasi-steady interaction domain near the surface is accompanied by a more favorable pressure gradient. As a result, the surface boundary layer downstream of this domain becomes thinner, allowing the flow to overcome stronger adverse pressure gradients and therefore delaying (or altogether suppressing) flow separation. The utility of synthetic jets for flow control was first demonstrated in the vectoring of conventional jets in the absence of extended control surfaces by Smith and Glezer[9] and in more detail by Smith.[10] Since then, this approach to flow control has been adopted in a number of other applications, including the modification of the aerodynamic characteristics of bluff bodies,[11,12] control of lift and drag on airfoils,[13] reduction of skin friction of a flat plate boundary layer,[14] mixing in circular jets,[15] control of internal flow separation,[16] and control of cavity oscillations.[17]

As noted by Smith and Glezer,[1] the instantaneous pressure field in the vicinity of the exit plane of a synthetic jet is substantially modified by the alternate, time-periodic entrainment and vortex formation and, as a result, the linear momentum of the jet decreases within a finite domain downstream of its exit plane. This unsteady evolution of the jet flow was exploited by Smith and Glezer to induce controlled interactions between two adjacent jets. The authors showed that when two high-aspect-ratio jets are placed side by side, parallel along the lengths of their orifices and spaced about one jet-width apart, the resultant jet can be dynamically manipulated by varying the amplitudes or the relative phase of the driving waveforms. The modification of the evolution of the vortex pairs that form each of the adjacent jets can lead to vectoring of the combined jet as demonstrated in the schlieren images of Figs. 1a and 1b. In these images, the driving signals have the same frequency and amplitude.

Presented as Paper 99-0669 at the AIAA 35th Aerospace Sciences Meeting, Reno, NV, 1 January 1999; received 18 August 2004; revision received 28 February 2005; accepted for publication 22 March 2005.

*Assistant Professor, Department of Mechanical and Aerospace Engineering.
†Professor, Woodruff School of Mechanical Engineering. Associate Fellow AIAA.

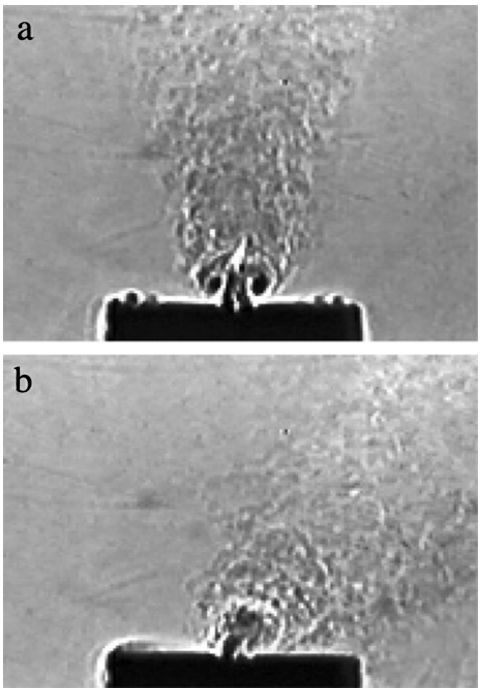

Fig. 1 Schlieren visualization of adjacent synthetic jets in the (x, y) plane for θ = a) 0 and b) 60 deg.

When the two jets are driven in phase (Fig. 1a), the inner vortices of each vortex pair cancel each other, resulting in a single, wider synthetic jet. However, when the driving signal of the jet on the right is leading in phase (by 60 deg, Fig. 1b), the pressure gradients induced by the blowing and suction strokes of the adjacent actuators and the interactions between the vortex pairs that form each jet lead to vectoring of the combined jet. In Fig. 1b, the vortex pair of the jet on the right is formed first while the neighboring actuator is still going through its suction stroke. The interaction between the adjacent vortex pairs (which are no longer aligned horizontally) and the flow that is induced by the jet actuators alters the vortex pair trajectories and, as a result, the merged jet is vectored toward the actuator that is leading in phase. More recently, phase interactions between adjacent spanwise rectangular jets were used by Holman et al.[18] to manipulate the aerodynamic performance of a NACA-0025 airfoil. These authors showed that when the airfoil is stalled, the flow can be reattached using the jet pair, and that the attachment was effectively independent of the phase.

The present investigation focuses on the flow mechanisms of the interaction between a pair of adjacent, high-aspect-ratio rectangular synthetic jets when the distance between the orifices is approximately twice the orifice width. A preliminary version of this work was reported in an earlier paper by Smith et al.[19] The two-jet apparatus and experimental procedure are described in Sec. II. The velocity fields of a single jet produced by the present setup and of the adjacent jets (driven in phase) are discussed in Sec. III, and form the baseline data for measurements of the flowfield of jets that are driven at prescribed phase differences in Sec. IV.

II. Experimental Apparatus and Procedure

The design of the present jet actuators is similar to the actuator that was used in the earlier work of Smith and Glezer.[2] The present generator comprises two adjacent cavities that are each driven independently by piezoelectric disks and are separated by a partition that also forms one of the long sides (75 mm) of each rectangular orifice. The width of each orifice is $h = 0.51$ mm, whereas the distance between the jet centerlines is $3.3h$, and the thickness of the orifice plate is $2.5h$, as shown schematically in Fig. 2. Each cavity is instrumented with a pressure transducer having a range of 1 psid and a frequency response of 100 kHz. The two-dimensionality of the actuator jet is confirmed by hot-wire anemometry at the slot exit.

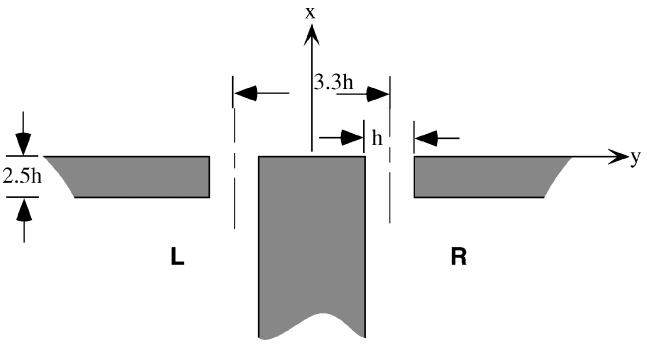

Fig. 2 Schematic diagram of the exit plane of the jet actuators.

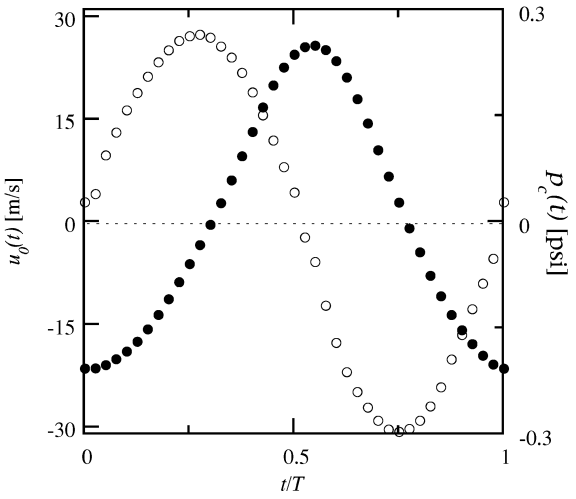

Fig. 3 Calibration of one of the adjacent jet actuators. The exit velocity (closed symbols) is calibrated with respect to the cavity pressure (open symbols) rather than input voltage and therefore holds even if the driver performance degrades or is replaced.

The piezoelectric disks that drive each jet are operated near resonance and their displacement is controlled by the amplitude of the time-harmonic driving signal. The motion of the disks results in a nominally time-harmonic streamwise orifice velocity $u_0(t)$ having amplitude U and zero mean within the orifice. Calibration curves that show the dependence of U on the cavity pressure amplitude in each generator are determined by placing a hot-wire sensor at the center of the orifice and simultaneously measuring the instantaneous velocity and cavity pressure phase-locked to the driving signal. These data are used to set the orifice speed during particle image velocimetry (PIV) measurements (calibration based on the driving voltage alone was found to be unreliable). A plot of a pressure/velocity calibration for a single two-dimensional jet ($U = 28$ m/s) is shown in Fig. 3 (the rectification of the velocity traces by the hot-wire sensor is removed). Time is normalized by the forcing period T so that $t^* = t/T$. For adjacent jets, t^* is based on the left-side actuator and $t^* = 0$ corresponds to the beginning of the blowing portion of the cycle. For the purposes of this calibration, it is assumed that the velocity profile in the orifice is uniform. Although the calibration does not depend on the drivers, it is very sensitive to frequency, to changes in the pressure near the jet exit plane, and to orifice geometry. In particular, when the jets are operated side by side, the velocity in each orifice is influenced by the presence of the adjacent jet and even more so when the phase between the two driving signals varies. Thus, in the present investigations, the Reynolds number of each of the adjacent jets is fixed at 300, and the cavity pressures that are needed to maintain this Reynolds number over the entire range of phase angles are determined iteratively. The reported phases are prescribed by a signal generator. The instantaneous pressure values in each cavity are monitored to confirm the input phase.

Following the notation of Smith and Glezer,[2] in the present work the synthetic jets are characterized using two primary dimensionless parameters. These parameters are the dimensionless "stroke" length L_0/h, which is based on a simple "slug" model where

$$L_0 = \int_0^{T/2} u_0(t)\,\mathrm{d}t$$

$u_0(t)$ is the centerline velocity, $T/2$ is the time of discharge, and the jet Reynolds number $Re = U_0 h/\nu = L_0 h/T\nu$, where $U_0 = L_0/T$.

The velocity field of the synthetic jets in the present experiments was measured using PIV. The experiments were performed inside a sealed glass enclosure measuring $86 \times 61 \times 41$ cm (x, y, and z directions, respectively). The flow was seeded using either theater fog or incense smoke and planar sections were illuminated using a double-pulse (8 μs apart) ND-YAG laser, phase-locked to the driving signal. Image pairs were captured using a 1000×1000 pixel CCD camera with a magnification of 20 μm/pixel. Velocity vectors are generated using a standard cross-correlation technique and computed using a square interrogation spot measuring 32 pixels on the side on a 64×64 grid with spacing of $0.63h$. At least 50 realizations are phase-averaged at 36 equally spaced intervals during the actuator cycle (or period T), where the measurement time is referenced to the beginning of the blowing stroke. Based on turbulent fluctuations of 20% of the mean, the uncertainty of the mean quantities is estimated to be 3%. It should be noted that some spatial resolution was sacrificed to make the measurement domain large enough to capture the vectoring effects, and consequently the present measurements cannot fully resolve the high velocity gradients (and therefore vorticity and shear stress) near the jet exit. However, knowledge of the exact magnitude of vorticity distributions is not necessary to form the main conclusions of the present paper.

III. Single and Adjacent Synthetic Jets

The velocity fields of a single jet and of a pair of adjacent jets that are driven in phase (cf. Sec. II) are mapped within a square domain in the x–y plane $z = 0$, which is centered about the jet's centerline, measures $37.3h$ on a side, and is bounded by the jet exit plane $x = 0$. The measurements are taken at jet Reynolds number $Re = 300$ and $L_0/h = 29$ (the jet actuation frequency is 600 Hz). Time-averaged streamline maps in the near field of the single and two-jet flows are shown in Figs. 4a and 4b, respectively. The contour increments are $0.223Q_0$, where $Q_0 = hL_0/T$ is the slug volume flow rate per unit span of the orifice. In these time-averaged maps, the volume flow rate through the jet orifice is clearly zero and the entrained fluid simply turns into the jet. This is not the case in phase-averaged streamline maps in which a time-dependent stagnation point appears on the jet centerline during the suction stroke of the actuator along with a stream surface that separates between the fluid that is entrained into the jet column and fluid layer that is drawn into the orifice.[9] The streamlines of a single jet (out of the left orifice in Fig. 2) exhibit a slight asymmetry about the orifice centerline. The slight tilting to the left is caused by the orifice asymmetry and the presence of the flow partition (Fig. 4a). Similarly, when the jet on the right side of the actuator in Fig. 2 is operated by itself, it is vectored to the right. When the left and right jets are operated simultaneously and in phase (Fig. 4b), the streamlines of the combined flow are reasonably symmetric about the generator's centerline and, as expected, the merged jet entrains more ambient fluid and transports a higher volume flow rate. The stronger entrainment of ambient fluid toward the jet orifice (as is evidenced by the angle of the streamlines on either side of the jet column) indicates that the pressure in the vicinity of the orifices is lower than when a single jet is operating. The (approximate) volume flow rate that is transported by the combined jet across the upper edge of the field of view (on one side of the centerlines) is slightly more than double the flow rate of the single jet; however, the width of the combined jet is clearly not twice the width of the single jet.

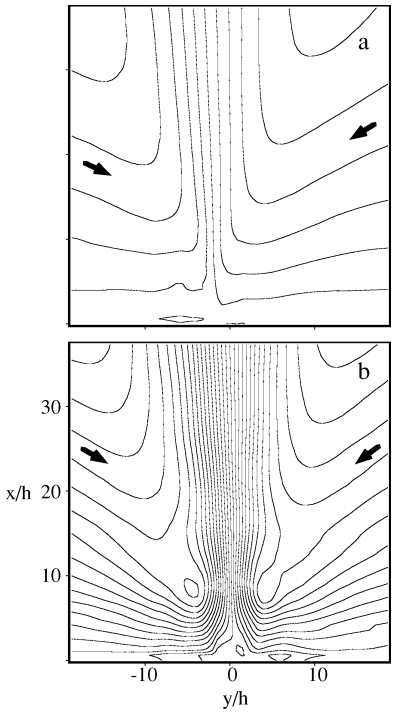

Fig. 4 Contour maps of the stream function of the mean flow ($Re = 300$; $L_0/h = 29$) for a) a single jet and b) adjacent jets. The contour increment is $0.223Q_0$.

Contours of the phase-averaged dimensionless spanwise vorticity $\langle\omega^*\rangle = \langle\omega\rangle L_0/U_0$ computed at four equally spaced time intervals during the actuation period are shown in Figs. 5a and 5b for the single jet and adjacent jets, respectively [negative, counterclockwise (CCW) vorticity is indicated by dashed lines]. At $t^* = t/T = 0.055$, the vortex sheets in the shear layers at the edges of each orifice are beginning to roll into a counter-rotating vortex pair (there are two adjacent vortex pairs in Fig. 5b.1). In each case, the remnants of vorticity concentrations from the previous actuation stroke are visible farther downstream. At the peak of the blowing stroke (Figs. 5a.2 and 5b.2), the new vortex pair that is formed at each of the jet orifices has left the exit plane and begun to move downstream. The presence of vorticity concentrations in the wake behind the vortex pair in Fig. 5a.2 suggests that the vortices of the single jet are advected downstream before the entire vortex sheet is rolled about the core. This means that circulation about the vortex core is actually lower than the total circulation that is imparted during the formation stroke.[20] Owing to interactions with the outer vortices, it appears that the cores of the center (inner) vortices in Fig. 5b.2 are beginning to stretch in the streamwise direction. Whereas these interactions are reminiscent of the dynamics of "leapfrogging" in two-dimensional and axisymmetric conventional jets, it is important to recognize that in the present configuration, the self-induced velocity of the center vortex pair is actually toward the jet orifice. While the speed (or the celerity) of the vortex cores in a single jet scales with the stroke length,[2] Fig. 5b.2 suggests that the celerity (characteristic speed) of the vortex cores of the adjacent jets is somewhat lower than in the single jet (Fig. 5a.2) ostensibly due to the interactions between the "inner" and "outer" vortex pairs. Furthermore, the cross-stream width of the domain that contains appreciable concentrations of vorticity downstream of the main vortices ($x/h > 10$) is nominally the same for both the single jet and the jet pair, suggesting that the interactions between the vortices of the adjacent jets result in rapid cancellation and diffusion of vorticity.

It is noteworthy that even though the suction into the orifice has not commenced, the flow induced by the vortex cores near the surface of the actuators exit plane leads to the formation of vorticity concentrations of opposite sense that are associated with the formation of a surface boundary layer. These concentrations are further intensified following the onset of suction (Figs. 5a.3 and 5b.3), although

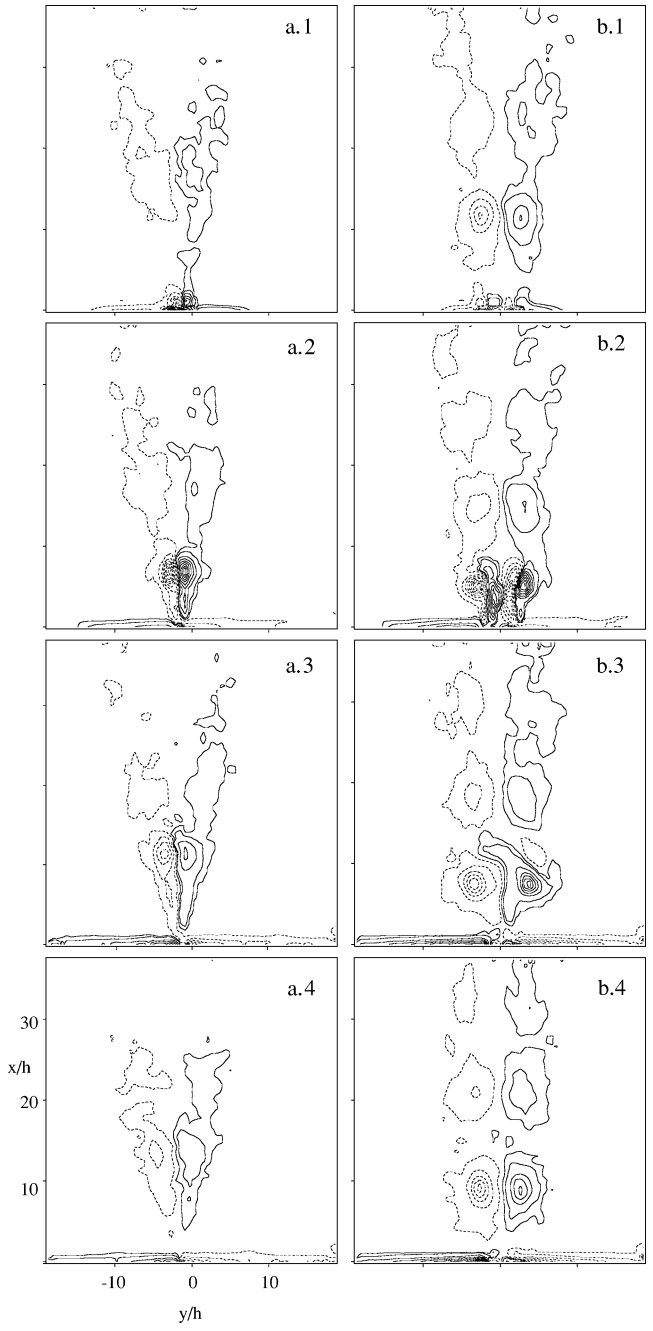

Fig. 5 Contours of the phase-averaged (dimensionless) spanwise vorticity $\langle\omega^*\rangle$ at $t^* = 0.055$, 0.278, 0.528, and 0.778 for (a.1–a.4) single jet and (b.1–b.4) adjacent jets (negative, CCW vorticity is indicated by dashed lines). Contour levels begin at ± 0.057, the next level is ± 0.071, and thereafter, the contour increments are ± 0.0142.

vorticity levels within the wall boundary layers of the jet pair are higher than those for the single jet, indicating a stronger flow along the wall. Because each jet in the pair entrains fluid from one side, the flow rate on each side is double the flow induced by the single jet. As shown in Figs. 5a.3 and 5b.3, the vortices of the merged jet pair evolve into a single pair of counter-rotating vortices that are closer to the generator orifice than the vortex pair of the single jet (and therefore may be further slowed by the suction). It is also noted that the vortices of the merged jet appear to remain more coherent at the later stages of the actuation cycle (Figs. 5a.4 and 5b.4) despite their interactions with the inner vortices.

The streamwise evolutions of the single jet and of the merged jet pair in terms of the decay of their centerline velocities and the variation of their flow rates (Figs. 6 and 7, respectively) are compared by scaling the streamwise coordinate with the total orifice width

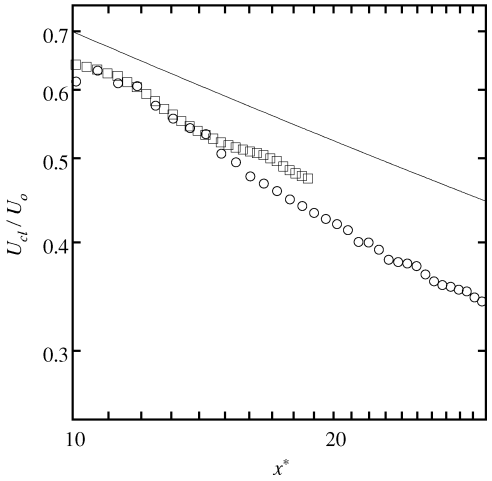

Fig. 6 Streamwise variation of centerline velocity for ○, a single jet and □, adjacent jets. The solid line is $x^{-1/2}$.

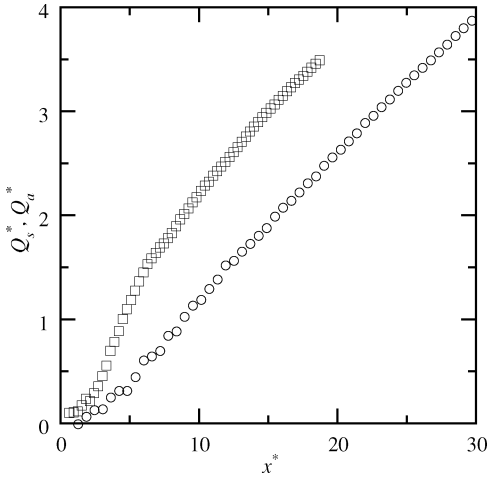

Fig. 7 Streamwise variation of volume flow rate for ○, a single jet and □, adjacent jets.

(i.e., $x^* = x/h$ and $x/2h$ for the single jet and for the adjacent jets, respectively). Although near the exit plane ($x^* < 15$) the (scaled) streamwise velocity of the jet pair is almost identical to that of the single jet, (even though the flowfields there are quite different), at $x^* = 19$ the velocity of the merged jet pair is about 10% higher than in the single jet. It appears that the lower streamwise decay rate of the characteristic velocity of the merged jet pair compared to the single jet is related to the slower decay of the merged vortex pairs (cf. Fig. 5). It is interesting to note that the decay rate of the jet pair is closer to that of a conventional two-dimensional turbulent jet ($x^{-0.5}$, shown for comparison). The normalized volume flow rates $Q_s^* = Q/Q_0$ for a single jet and $Q_a^* = Q/2Q_0$ for the adjacent jets (Fig. 7) show that for $x^* > 6$, the volume rates of both flows vary almost linearly with x^*, although the merged jet pair grows at a larger streamwise rate (about 2.5 times as fast for $x^* < 6$, and about 10% higher for $x^* > 10$). The fast increase in entrainment in the near field of the jet pair is apparently associated with the dynamics of vortex merging. When vortex interactions of the adjacent jets are complete ($x^* > 6$), the streamwise entrainment rate decreases.

IV. Adjacent Synthetic Jets at Varying Phase Angles

As shown in Fig. 1 (see also Smith and Glezer[2,8]), when two adjacent synthetic jets are driven so that there is a phase difference between the two driving signals, the combined jet vectors toward the actuator that is leading in phase. The variation of the vectoring with the phase difference is demonstrated in a sequence of time-averaged streamline maps in Fig. 8 in the x–y plane, $z = 0$, where the actuator

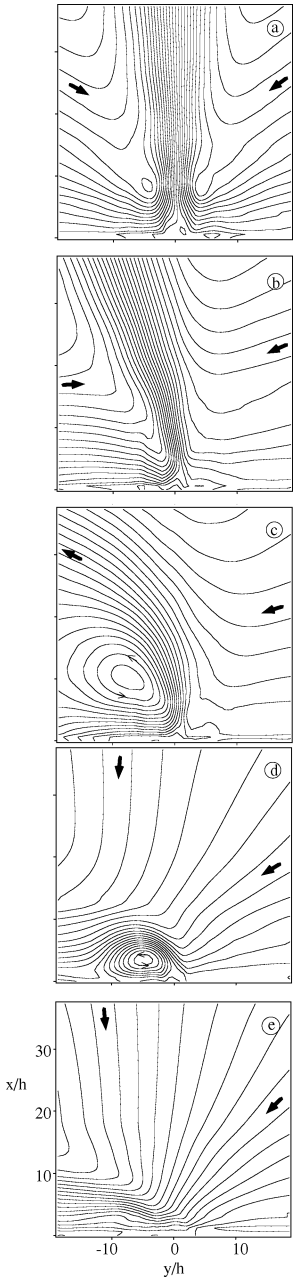

Fig. 8 Contour maps of the time-averaged stream function for adjacent jets: θ = a) 0, b) 60, c) 70, d) 80, and e) 130 deg. The contour increment is $0.223Q_0$.

on the left is leading in phase (the phase angle between the jets is θ). The contour increments are $0.223\,Q_0$ (as in Fig. 4).

In Fig. 8a (which is identical to Fig. 4b), the two jets are in phase (i.e., $\theta = 0$). The combined jet is symmetric about the centerline $y = 0$, and the entrained flow across $y/h = \pm 18$ (i.e., the left and right edges of the measurement domain) is directed toward the jet orifices. The spacing between these streamlines and their inclination relative to the jets exit plane $x = 0$ decrease with x indicating that the entrainment speed increases with proximity to the exit plane. As noted in connection with Fig. 4, the time-averaged entrained flow turns in the streamwise direction within the jets because there is now net flow into the orifices. When $\theta = 60$ deg (Fig. 8b), the merged jet is vectored to the left (i.e., toward the jet that is leading in phase) at an angle nominally of 17 deg (relative to $y = 0$). The entrained flow into the jet column is asymmetric and, as is evidenced by the number and spacing of the streamlines, the volume flow rate of entrained fluid is clearly larger on the left (by almost 33% through $0 < x/h < 36$ at $y/h = \pm 18$). However, the overall entrainment (e.g., compared to $\theta = 0$) is about the same.

As shown by Smith et al.,[19] the time-averaged streamline maps change substantially when $\theta = 70$ deg (Fig. 8c) with the formation of a closed circulation region on the left. When the phase angle between the adjacent jets is increased further ($\theta = 80$ deg, Fig. 8d), a confined circulation domain is formed between the combined jet and the exit plane and the jet is effectively attached to the surface on the left.

Judging by the streamline pattern at the left edge of the flow domain in Fig. 8d, the volume flow rate of fluid that is transported by the merged jet is considerably smaller in this phase because a significant part of the jet fluid is recirculating near the orifices. This pattern continues as the phase angle exceeds 90 deg and the recirculation domain becomes much smaller, presumably because the flow is confined to the vicinity of the orifices (e.g., Fig. 8e, $\theta = 130$ deg). Finally, when the phase angle is close to 180 deg (not shown), the instantaneous flow is predominantly characterized by alternating flows out of and into the adjacent cavities with relatively weak, featureless time-averaged flow. Although most of the vortices that are formed at the orifices become trapped in the alternating flow between the orifices, slight mismatches between the drivers and the jet cavities can lead to random ejection and advection of some vortical structures.

The evolution of the adjacent jets at several phases that characterize the different interaction regimes is investigated in more detail using phase-averaged vorticity concentrations that are computed from PIV measurements. These interactions can be roughly divided into three primary regimes, namely, free vectoring ($\theta < 70$ deg), vectored flow with a recirculating flow domain (80 deg $< \theta <$ 100 deg), and nominally attached flow ($\theta > 110$ deg). In what follows, these regimes are represented by contour maps of the phase-averaged dimensionless vorticity $\langle \omega^* \rangle$ that are measured in the streamwise domain $x/h < 20$ at four phase angles, $\theta = 0$, 60, 80, and 130 deg. These vorticity maps are measured phase-locked to the actuation waveform and at dimensionless time $t^* = t/T$ relative to the onset of the blowing cycle of the actuator that is leading in phase (i.e., $t^* = 0$ and 0.5 correspond to the beginning of the blowing and suction cycles of the leading actuator, respectively). Contour levels begin at $\langle \omega^* \rangle = \pm 0.071$, and the contour increments are ± 0.142. The notation that is used for discussing these data is shown schematically in Fig. 9, where the counter-rotating vortex pairs from the left (L) and right (R) actuators are marked by L^-, L^+, and R^-, R^+ [clockwise (CW) vorticity is taken to be positive]. The merged vortex pair is referred to as M^+ and M^-. It is important to recognize that the vortices that are formed during the time-periodic ejection of fluid from each orifice are, in fact, advected in a velocity field that is largely dominated by the alternating blowing and suction cycles of the actuators. This velocity field clearly affects the interactions between the vortices and the ultimate structure and trajectories of the merged jets.

Figure 10 shows a sequence of eight contour maps of phase-averaged vorticity distributions in the x–y plane for $\theta = 0$ deg (beginning at $t^* = 0.11$). In Fig. 10a, four vortices of approximately equal strength and alternating signs (i.e., L^-L^+, and R^-R^+) are simultaneously formed near the exit plane, whereas the combined pair from the previous cycle (M^-M^+) is visible near $x/h \approx 12$. By $t^* = 0.17$, the two pairs appear to increase in strength and are advected downstream of the jet orifices. As the advection continues ($t^* = 0.22$), the cross sections of the vortices appear to stretch in the streamwise direction. The interaction between the vortex pairs is such that whereas the self-induced motion of the outer vortex pair

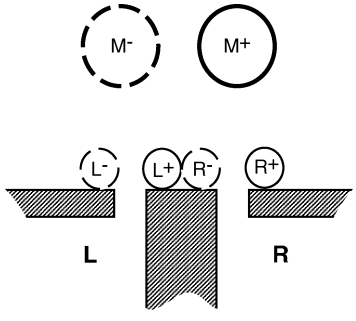

Fig. 9 Schematic diagram of the vortices generated by adjacent synthetic jets.

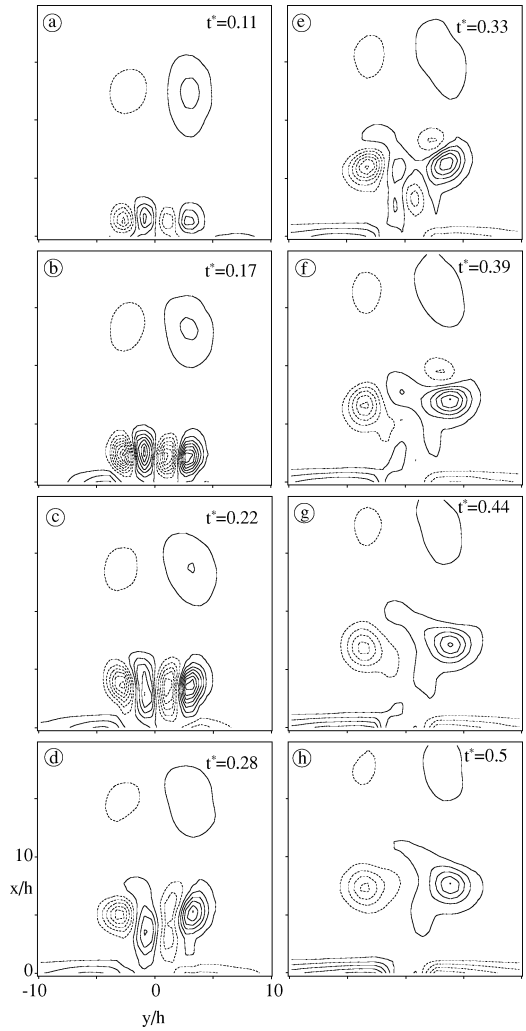

Fig. 10 Contour maps of $\langle\omega^*\rangle$ for $\theta = 0$ at t^* = a) 0.11, b) 0.17, c) 0.22, d) 0.28, e) 0.33, f) 0.39, g) 0.44, and h) 0.5. The first contour level is ± 0.071 and the contour increments are ± 0.142.

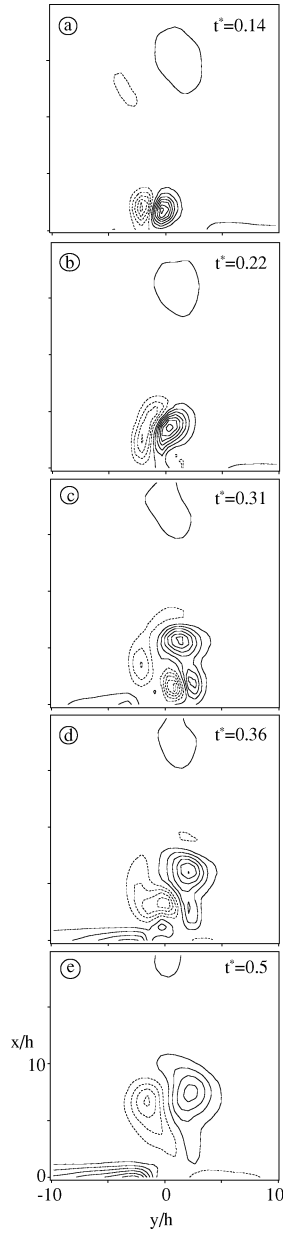

Fig. 11 Contour maps of $\langle\omega^*\rangle$ for $\theta = 60$ deg at t^* = a) 0.14, b) 0.22, c) 0.31, d) 0.36, and e) 0.5. The contour increments are the same as in Fig. 10.

(i.e., L^-R^+) is in the downstream direction, the center pair (i.e., L^+R^-) tends to advect toward the jet orifice. However, this motion is opposed by the streamwise motion of fluid that is still ejected from the orifice. When $t^* = 0.28$, the downstream edges of the cores of the inner vortices begin to wrap around the cores of the outer vortices and this wrapping (and subsequent ingestion and cancellation) is almost complete by $t^* = 0.39$. It is also noteworthy that the flow that is induced by the outer vortex pair (which ultimately forms the merged pair M^-M^+ in Fig. 10g) along the jet exit plane toward the orifices (e.g., Fig. 10c) forms boundary layers with opposite sense vorticity concentrations on both sides of the orifices. When the suction cycle begins (i.e., $t^* > 0.5$), these boundary layer flows become stronger, but the merged vortex pair is far enough removed from the exit so that its evolution is not substantially affected.

As shown in Fig. 8, when one of the adjacent actuators is leading in phase, the merged jet begins to tilt toward the leading actuator. The details of the vortex interactions that are associated with this vectoring are shown in Figs. 11a–11e ($\theta = 60$ deg). Because the actuator on the left is leading in phase (by $t^* = 1/6$), the pair L^-L^+ is formed ahead of the pair R^-R^+. In Fig. 11a ($t^* = 0.14$) the merged and tilted vortex pair from the previous cycle is still visible near $x/h = 0.15$ and a new vortex pair L^-L^+ is formed by the left actuator. The vortex L^+ is apparently stronger than L^- (as is evident from the vorticity concentration). This pair is beginning to form while the actuator on the right is in its suction cycle, and it appears that the induced flow by the suction tilts the momentary jet out of the left actuator to the right and therefore intensifies the vorticity in L^+ during its rollup. The L^-L^+ vortex pair in Fig. 11b ($t^* = 0.22$) is tilted to the right as it is advected away from the orifice and L^- is beginning to wrap around L^+. The pair R^-R^+ (which begins to form at $t^* = 0.17$) is visible in Fig. 11c, $t^* = 0.31$. The merging of the CCW vortices L^- and R^- apparently results in tilting of the pair M^+M^- to the left and induces the formation of a wall boundary layer on the left (Fig. 11d, $t^* = 0.36$). By the time the suction cycle of the left actuator is about to commence ($t^* = 0.5$, Fig. 11e), the merged vortex pair is already far enough removed and simply continues to be tilted and advected in the direction of the mean flow, which is along the axis of M^+M^-.

As noted in connection with Fig. 8d, the streamlines of the time-averaged flow suggest that when θ exceeds 70 deg, a closed recirculation domain is formed near the left side of the exit plane. Figure 12 ($\theta = 80$ deg) indicates that, at this phase angle, most of the vortex interactions are confined to the streamwise domain $x^* < 10$ and that the recirculation domain is associated with trapping of the vortex M^- on the left side of orifices and weakening of M^+. In Fig. 12a at $t^* = 0.11$, similarly to Fig. 10, a new vortex pair L^-L^+ is formed by the left actuator, while the merged vortex pair from the previous cycle is tilted (almost normal to the exit plane) near $y/h = -7$. As the blowing cycle of the left jet continues (as in Fig. 10, the vortex L^- is weaker owing to the suction into the right actuator), the vortex M^- is drawn toward the jet orifice, while M^+ continues its

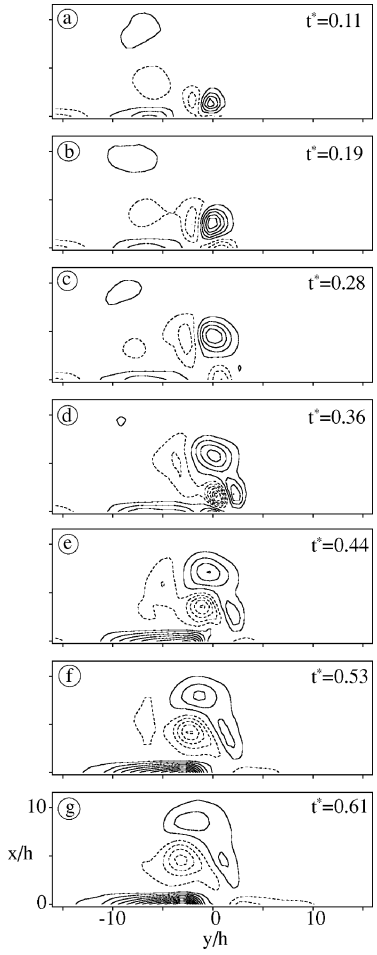

Fig. 12 Contour maps of $\langle\omega^*\rangle$ for $\theta = 80$ deg at $t^* =$ a) 0.11, b) 0.19, c) 0.28, d) 0.36, e) 0.44, f) 0.53, and g) 0.61. The contour increments are the same as in Fig. 10.

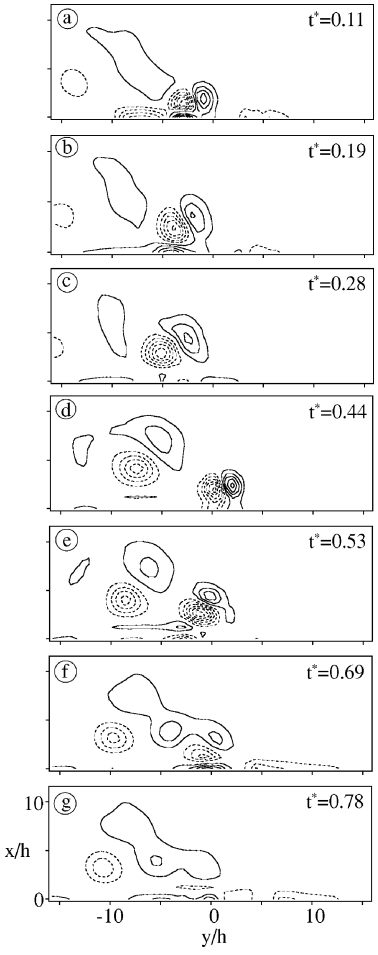

Fig. 13 Contour maps of $\langle\omega^*\rangle$ for $\theta = 130$ deg at $t^* =$ a) 0.11, b) 0.19, c) 0.28, d) 0.448, e) 0.53, f) 0.69, and g) 0.78. The contour increments are the same as in Fig. 10.

advection (Fig. 12b, $t^* = 0.19$). The presence of the CCW vorticity concentrations near the exit plane leads to the formation of CW vorticity at the surface, which intensifies as the new R^- vortex is formed (Fig. 12d, $t^* = 0.36$) and is advected to the left (Fig. 12e, $t^* = 0.44$). The cross-stream (i.e., y-direction) extent of this vorticity concentration is limited and is consistent with the formation of the recirculation domain of the time-averaged flow. It is noteworthy that the merged vortex pair is primarily dominated by L^+ and R^- and the line that connects between the centers of the cores of these vortices continuously tilts to the left as the formation and merging processes continue. The last two maps, Figs. 12f and 12g ($t^* = 0.53$ and 0.61, after the suction cycle of the left actuator begins), indicate that unlike the vorticity concentrations in Fig. 10, the merged vortices in Fig. 12 appear to remain in the vicinity of the orifices and there is no migration of coherent vorticity concentrations into the merged jet.

Finally, phase-averaged vorticity maps for $\theta = 130$ deg are shown in Figs. 13a–13g. The streamlines of the time-averaged flow show that in this phase, the merged jet is vectored to the left along the surface of the exit plane and the size of the recirculating flow domain that is present at lower phase angles is substantially diminished as a result of cross flow between the two adjacent actuators. At this phase angle, the vortex pairs L^-L^+ and R^-R^+ are separated by $\Delta t^* = 0.36$. In Fig. 13a ($t^* = 0.11$), the vortex pair L^-L^+ is already partially formed and L^- is somewhat stronger than L^+, ostensibly due to the presence of a cross flow to the left (cf. Fig. 8e). The presence of this cross flow is also evidenced by the layer of CCW vorticity along the left surface (through $y/h = -10$), indicating the presence of a wall boundary layer. As a result of the cross flow (and the stronger L^-) the vortex pair begins to tilt to the left (Fig. 13b, $t^* = 0.19$) following its formation. Note the formation of CW vorticity underneath L^-. It is also interesting to note that L^+ continues to weaken as it is sheared by the predominantly left-moving cross flow, although the rising of the vortex pair above the surface weakens the induced boundary layer on the left wall (e.g., Fig. 13c, $t^* = 0.28$). By the time the pair R^-R^+ begins to emerge ($t^* = 0.44$ in Fig. 13d), L^-L^+ is far enough removed and there is virtually no direct interaction between the two successive pairs. Similarly to L^-, R^- is also stronger than R^+ owing to the cross flow. The pair R^-R^+ continues to be tilted and advected to the left (Fig. 13e, $t^* = 0.53$) but apparently is influenced by the onset of suction into the orifice on the right, which forces R^- to migrate closer to the orifice (Fig. 13f, $t^* = 0.69$). By $t^* = 0.78$ (Fig. 13g), the vortices L^+ and R^+ are more or less merged and quite weak, whereas L-continues to be advected to the left.

V. Conclusions

The formation, evolution, and interactions of coflowing, adjacent, plane synthetic jets are investigated using PIV. The jets are placed side by side, so that they are parallel along the long dimension of their orifices. The actuation frequencies of the two jets are matched and because each actuator is independently driven, it is possible to vary the relative phase between the driving signals. It is shown that when the two jets are driven in phase, the volume flow rate of the entrained fluid on each side of the merged jet (and of the fluid that is transported by the merged jet) is more than double that of a single jet, whereas the centerline velocity is the same. When the phase angle between the actuation waveforms of the two jets is altered so that there is a delay between the suction and blowing cycles of the adjacent actuators, the merged jet is tilted (vectored) toward the jet that is leading in phase. The degree of vectoring increases with the phase angle until the merged jet flows along the surface of the exit plane. Maps of the time-averaged streamlines indicate that the vectored flow has three primary domains, which are characterized by the relative phase angle between the actuation waveforms, namely, free vectoring ($\theta < 70$ deg), vectored flow with a recirculating flow domain (80 deg $< \theta <$ 100 deg), and attached flow, where the recirculating flow domain is restricted to the vicinity of the orifices ($\theta > 110$ deg). The evolution of the adjacent jets at several phases that characterize the different interaction regimes

was investigated in detail using phase-averaged vorticity concentrations that are computed from PIV measurements. These data suggest that the vectoring of the merged jet depends critically on the timing (or phase differences) of the blowing and suction cycles and the flowfields and the time-varying pressure gradients that are induced by the oscillatory motion of fluid through the adjacent orifices. Furthermore, the evolution, the interactions, and ultimately the trajectories of the vortices that are formed by fluid ejection from each orifice are influenced by the global velocity field in the vicinity of the actuators.

At relatively low phase angles all the vortices of the vortex pair have nominally the same circulation and the inner vortices within the two pairs are effectively cancelled by the outer vortices. As the phase angle increases, the vortex pair of the jet that is leading in phase begins to be influenced by the adverse pressure gradient (and a corresponding velocity field) that is induced by the suction cycle of the adjacent jet. As a result, the circulations of the vortices of each pair are no longer the same, leading to complex interactions of the vortex pairs and their tilting relative to the jet axis until the jet becomes attached to the surface of the exit plane. When the phase angle exceeds 120 deg, the successive vortex pairs do not merge and the pair that is lagging in phase begins to be influenced by the suction cycle at the adjacent orifice.

Acknowledgment

This work was supported by the Air Force Office of Scientific Research.

References

[1]Smith, B. L., and Glezer, A., "Vectoring and Small-Scale Motions Effected in Free Shear Flows Using Synthetic Jet Actuators," AIAA Paper 97-021, 1997.

[2]Smith, B. L., and Glezer, A., "The Formation and Evolution of Synthetic Jets," *Physics of Fluids*, Vol. 10, No. 9, 1998, pp. 2281–2297.

[3]Cater, J. E., and Soria, J., "The Evolution of Round Zero-Net-Mass-Flux Jets," *Journal of Fluid Mechanics*, Vol. 472, 1997, pp. 167–200.

[4]Smith, B. L., and Swift, G. W., "A Comparison Between Synthetic Jets and Continuous Jets," *Experiments in Fluids*, Vol. 34, No. 4, 2003, pp. 467–472.

[5]Kral, L. D., Donovan, J. F., Cain, A., and Cary, A. W., "Numerical Simulation of Synthetic Jet Actuators," AIAA Paper 97-1824, 1997.

[6]Rizzetta, D. P., Visbal, M. R., and Stanek, M. J., "Numerical Investigation of Synthetic-Jet Flowfields," *AIAA Journal*, Vol. 37, No. 8, 1999, pp. 919–927.

[7]Honohan, A. M., Amitay, M., and Glezer, A., "Aerodynamic Control Using Synthetic Jets," AIAA Paper 2000-2401, 2000.

[8]Glezer, A., Amitay, M., and Honohan, A. M., "Aspects of Low- and High-Frequency Aerodynamic Flow Control," *AIAA Journal*, Vol. 43, No. 7, 2005, pp. 1501–1511.

[9]Smith, B. L., and Glezer, A., "Jet Vectoring Using Synthetic Jets," *Journal of Fluid Mechanics*, Vol. 458, 2002, pp. 1–34.

[10]Smith, B. L., "Synthetic Jets and Their Interaction with Adjacent Jets," Ph.D. Dissertation, Woodruff School of Mechanical Engineering, Georgia Inst. of Technology, Atlanta, June 1999.

[11]Amitay, M., Smith, D. R., Kibens, V., Parekh, D., and Glezer, A., "Aerodynamic Flow Control of Bluff Bodies Using Synthetic Jets Technology," *Mechanics of Passive and Active Flow Control (IUTAM)*, edited by G. E. A. Meier and P. R. Viswanath, Kluwer Academic, Dordrecht, The Netherlands, 1998, pp. 273–278.

[12]Amitay, M., Smith, B. L., and Glezer, A., "Aerodynamic Flow Control Using Synthetic Jet Technology," AIAA Paper 98-0208, 1998.

[13]Amitay, M., Smith, D. R., Kibens, V., Parekh, D., and Glezer, A., "Aerodynamic Flow Control of an Unconventional Airfoil Using Synthetic Jet Actuators," *AIAA Journal*, Vol. 39, No. 3, 2001, pp. 361–370.

[14]Rathnasingham, R., and Breuer, K. S., "Active Control of Turbulent Boundary Layers," *Journal of Fluid Mechanics*, Vol. 495, 2004, pp. 209–233.

[15]Davis, S., and Glezer, A., "Manipulation of Large- and Small-Scales in Coaxial Jets Using Synthetic Jet Actuators," AIAA Paper 2000-0403, 2000.

[16]Amitay, M., Pitt, D., and Glezer, A., "Separation Control in Duct Flows," *Journal of Aircraft*, Vol. 39, No. 4, 2002, pp. 616–620.

[17]Fabris, D., and Williams, D. R., "Experimental Measurements of Cavity and Shear Layer Response to Unsteady Bleed Forcing," AIAA Paper 99-0605, 1999.

[18]Holman, R., Gallas, Q., Carroll, B., and Cattafesta, L., "Interaction of Adjacent Synthetic Jets in an Airfoil Separation Control Application," AIAA Paper 2003-3709, 2003.

[19]Smith, B. L., Trautman, M. A., and Glezer, A., "Controlled Interactions of Adjacent Synthetic Jets," AIAA Paper 99-0669, 1999.

[20]Gharib, M., Rambod, E., and Shariff, K., "A Universal Time Scale for Vortex Ring Formation," *Journal of Fluid Mechanics*, Vol. 360, 1998, pp. 121–140.

H. Reed
Associate Editor